Testing the scalar triplet solution to CDF's heavy W problem at the LHC

Jon Butterworth,[1,*] Julian Heeck,[2,†] Si Hyun Jeon,[3,‡] Olivier Mattelaer,[4,§] and Richard Ruiz[5,‖]

[1]*Department of Physics and Astronomy, University College London, Gower Street, London, WC1E 6BT, United Kingdom*
[2]*Department of Physics, University of Virginia, Charlottesville, Virginia 22904-4714, USA*
[3]*Department of Physics and Astronomy, Seoul National University, 1 Gwanak-Ro, Gwanak-gu, Seoul, 08826, Korea*
[4]*Centre for Cosmology, Particle Physics and Phenomenology (CP3), Université catholique de Louvain, Chemin du Cyclotron, Louvain-la-Neuve, B-1348, Belgium*
[5]*Institute of Nuclear Physics—Polish Academy of Sciences (IFJ PAN), ul. Radzikowskiego, Kraków, 31-342, Poland*

(Received 23 December 2022; accepted 8 March 2023; published 18 April 2023)

The type II seesaw model remains a popular and viable explanation of neutrino masses and mixing angles. By hypothesizing the existence of a scalar that is a triplet under the weak gauge interaction, the model predicts strong correlations among neutrino oscillation parameters, signals at lepton flavor experiments, and collider observables at high energies. We investigate reports that the type II seesaw can naturally accommodate recent measurements by the CDF collaboration, which finds the mass of the W boson to be significantly larger than allowed by electroweak precision data, while simultaneously evading constraints from direct searches. Experimental scrutiny of this parameter space in the type II seesaw has long been evaded since it is not characterized by "golden channels" at colliders but instead by cascade decays, moderate mass splittings, and many soft final states. In this work, we test this parameter space against publicly released measurements made at the Large Hadron Collider. By employing a newly developed tool chain combining MadGraph5_AMC@NLO and CONTUR, we find that most of the favored space for this discrepancy is already excluded by measurements of Standard Model final states. We give suggestions for further exploration at run III of the LHC, which is now under way.

DOI: 10.1103/PhysRevD.107.075020

I. INTRODUCTION

In April 2022, the CDF collaboration at Fermilab reported its legacy measurement of the W boson's mass (M_W) using $\mathcal{L} = 8.8\ \text{fb}^{-1}$ of $p\bar{p}$ collision data at $\sqrt{s} = 1.96$ TeV from the Tevatron using the so-called template method [1]. At a value of

$$M_W^{\text{CDF}} = 80.4335\ \text{GeV} \pm 9.4\ \text{MeV}, \tag{1}$$

this precision measurement exceeds by many standard deviations both the presently accepted LEP2 + Tevatron average of [2]

$$M_W^{\text{LEP2+Tev}} = 80.385\ \text{GeV} \pm 15\ \text{MeV} \tag{2}$$

and the LEP2 + Tevatron + LHC[1] "world average" of [5]

$$M_W^{\text{World 2021}} = 80.379\ \text{GeV} \pm 12\ \text{MeV}, \tag{3}$$

which are predicted in the Standard Model (SM) by electroweak (EW) precision data (EWPD). Importantly, studies so far show that improvements in parton density functions [6] and perturbative matrix elements [7,8] cannot account for this large discrepancy. However, some SM explanations remain unexplored. For example, the difference may be due to high-twist power corrections that are normally neglected in perturbative calculations [9–11].

*J.Butterworth@ucl.ac.uk
†heeck@virginia.edu
‡si.hyun.jeon@cern.ch
§olivier.mattelaer@uclouvain.be
‖rruiz@ifj.edu.pl

[1]The LHC contribution is solely from the ATLAS collaboration's run I measurement [3] and does not include LHCb's early run II measurement [4]. The CMS collaboration has not yet reported a measurement of M_W.

Alternatively, CDF's measurement of M_W is ultimately a one-parameter fit of the W boson's transverse mass. This distribution also depends on the W's width (Γ_W), and so a two-parameter fit of (M_W, Γ_W) may reveal a shift in Γ_W.

Since CDF's finding, numerous beyond the SM (BSM) solutions with varying complexity, novelty, and tenability have been proposed. One outlier among these scenarios is the type II seesaw model for neutrino masses [12–17], which has long predicted a shift in the W-to-Z mass ratio. The model is characterized by the existence of colorless scalars $\Delta^{\pm\pm}, \Delta^{\pm}, \Delta^0, \xi^0$ that (i) form a triplet ($\hat{\Delta}$) under the weak gauge interaction, (ii) carry lepton number, and (iii) couple to EW gauge bosons and leptons at tree level. More relevantly, after electroweak symmetry breaking (EWSB), $\hat{\Delta}$ acquires a vacuum expectation value (VEV) $v_\Delta = \sqrt{2}\langle\hat{\Delta}\rangle$ that reduces the W-to-Z mass ratio at tree level [18], but at one loop the mass splittings of multiplets can *increase* the ratio, and hence increase M_W [19,20].

Dedicated studies [21–25] point to an intriguing narrative [22]: a VEV above 1 MeV and scalar masses between $m_\Delta \sim 100$ and 300 GeV cannot only resolve CDF's contention with EWPD but also evade constraints from direct searches by the ATLAS [26–29] and CMS [30,31] collaborations at the Large Hadron Collider (LHC) as well as evade constraints from searches for lepton-flavor-violating decays of charged leptons.

In this study, we draw attention to the fact that the masses, mass splittings, and VEV needed for this resolution give rise to a complex collider phenomenology. In this regime, the type II seesaw is not characterized by so-called "golden channels" at colliders. Instead, the mass splittings and effective couplings are so large that the decays of triplet scalars are dominated by the decays to one or more (virtual or on-shell) weak bosons and lighter, unstable scalars [32–37]. While this weakens searches for triplet scalars decaying predominantly to lepton pairs or on-shell weak boson pairs, i.e., golden channels, it also leads to a multitude of processes with many final-state charged leptons, neutrinos, and jets possessing various kinematics. Assuming the findings of Refs. [21–23,25] are realized in nature, it follows that a multitude of measurements at the LHC, especially differential cross sections for multilepton production, contain contributions of some degree from type II scalars.

In light of this, we have investigated the constraining power of measurements of SM signatures from the LHC on the type II seesaw in the preferred parameter space identified by Ref. [22]. We employ a tool chain that interfaces MadGraph5_AMC@NLO (MGaMC) [38,39] and CONTUR [40,41], and which accesses the measurements from 161 publications from ATLAS, CMS, and LHCb. We use the CONTUR mode which accesses the SM predictions directly, as discussed in [42], and so of these papers, we use only the subset (46) for which SM predictions are currently available in CONTUR. In practice, only a handful of these analyses drive our results, as will be discussed in the relevant section. As a consequence, we definitively test a parameter space in the type II seesaws that, until now, escaped experimental scrutiny.

The remainder of this study continues as follows: In Sec. II we summarize the type II seesaw model, current experimental constraints, and best-fit parameter spaces. In Sec. III, we outline our methodology and the tools used. We present our results in Sec. IV. In Sec. V we conclude with an outlook for future work.

II. THEORETICAL FRAMEWORK

Throughout this study, we work in the framework of the type II seesaw model for neutrino masses [12–17]. This scenario extends the SM's field content by a single complex, scalar multiplet. In the gauge basis, this field is denoted by $\hat{\Delta}$ following the notation of Ref. [43]. Under the SM gauge group $\mathcal{G}_{\rm SM} = \mathrm{SU}(3)_c \otimes \mathrm{SU}(2)_L \otimes U(1)_Y$, the multiplet carries the gauge quantum numbers $(\mathbf{1}, \mathbf{3}, +1)$. This means that the individual states comprising $\hat{\Delta}$ are colorless but carry EW charges and couple to EW bosons via gauge couplings. The weak hypercharge and isospin charges are normalized such that the electromagnetic charge operator is $\hat{Q} = \hat{T}^3_L + \hat{Y}$. In terms of states with definite electric charge, $\hat{\Delta}$ and its VEV (v_Δ) are, respectively,

$$\hat{\Delta} = \begin{pmatrix} \frac{1}{\sqrt{2}}\hat{\Delta}^+ & \hat{\Delta}^{++} \\ \hat{\Delta}^0 & -\frac{1}{\sqrt{2}}\hat{\Delta}^+ \end{pmatrix} \quad \text{and} \quad \langle\hat{\Delta}\rangle = \frac{1}{\sqrt{2}}\begin{pmatrix} 0 & 0 \\ v_\Delta & 0 \end{pmatrix}. \tag{4}$$

The tree-level Lagrangian of the type II seesaw is given by

$$\mathcal{L}_{\text{Type II}} = \mathcal{L}_{\rm SM} + \mathcal{L}_{\text{Kin.}} + \mathcal{L}_{\text{Yukawa}} + \mathcal{L}_{\text{Scalar}}. \tag{5}$$

Here, $\mathcal{L}_{\rm SM}$ is the SM Lagrangian. $\mathcal{L}_{\text{Kin.}}$ is the kinetic term

$$\mathcal{L}_{\text{Kin.}} = \mathrm{Tr}[D_\mu\hat{\Delta}^\dagger D^\mu\hat{\Delta}], \tag{6}$$

wherein the covariant derivative for $\hat{\Delta}$ is

$$D_\mu\hat{\Delta} = \partial_\mu\hat{\Delta} - \frac{i}{2}g_W W^k_\mu[\sigma_k\hat{\Delta} - \hat{\Delta}\sigma_k] - ig_Y B_\mu\hat{\Delta}. \tag{7}$$

In the above, W^k_μ, with $k = 1, \ldots, 3$, are the weak gauge states before EWSB and couple to $\hat{\Delta}$ with a universal strength of $g_W \approx 0.65$. σ_k are the usual 2×2 Pauli matrices. B_μ is the weak hypercharge gauge state that couples with a strength of $g_Y = e/\cos\theta_W \approx 0.36$, where $\theta_W \approx 29°$ is the weak mixing angle.

The term $\mathcal{L}_{\text{Yukawa}}$ is the Yukawa interaction between $\hat{\Delta}$ and the left-handed SM leptons,

$$\mathcal{L}_{\text{Yukawa}} = -\mathbf{Y}_\Delta \bar{L}^c \hat{\Delta} L + \text{H.c.}, \tag{8}$$

where $\mathbf{Y}_\Delta$ is a complex symmetric 3×3 matrix of Yukawa couplings. Equation (8) conserves lepton number if we assign $L_\Delta = -2$ to $\hat{\Delta}$. After EWSB, the term generates Majorana masses for neutrinos and is given by the following in the flavor basis:

$$\mathcal{L}_{\text{Yukawa}} \ni \frac{v_\Delta}{\sqrt{2}} (\mathbf{Y}_\Delta)_{ff'} \overline{\nu^c_{Lf}} \cdot \nu_{Lf'} + \text{H.c.} \tag{9}$$

The prefactor corresponds to the neutrino mass matrix, which can be diagonalized by a unitary rotation. Diagonalizing allows us to express the Yukawa couplings in terms of the diagonal neutrino mass matrix m_ν^{diag} as well as the mixing angles and phases within the Pontecorvo-Maki-Nakagawa-Sakata matrix U^{PMNS}. In terms of these, the Yukawa coupling matrix is

$$\mathbf{Y}_\Delta = \frac{1}{\sqrt{2} v_\Delta} \left(U^{\text{PMNS}}\right)^* m_\nu^{\text{diag}} \left(U^{\text{PMNS}}\right)^\dagger, \tag{10}$$

The direct connection between oscillation parameters and Yukawa couplings implies that the decays of $\hat{\Delta}$'s components to leptons at high-energy colliders are correlated with neutrino oscillation data [33,34]. For predictions of correlations using up-to-date oscillation data, see Refs. [37,43]. Notice that even with full knowledge of neutrino masses and mixing parameters, the overall scale of $\mathbf{Y}_\Delta$ is degenerate with the magnitude of v_Δ.

Finally, the scalar potential $\mathcal{L}_{\text{Scalar}}$, which includes the self-couplings of $\hat{\Delta}$ and couplings of $\hat{\Delta}$ to the SM Higgs doublet φ before EWSB, is

$$\begin{aligned} -\mathcal{L}_{\text{Scalar}} = {} & m_{\hat{\Delta}}^2 \text{Tr}[\hat{\Delta}^\dagger \hat{\Delta}] + \lambda_{\Delta 1} (\text{Tr}[\hat{\Delta}^\dagger \hat{\Delta}])^2 + \lambda_{\Delta 2} \text{Tr}[(\hat{\Delta}^\dagger \hat{\Delta})^2] \\ & + \lambda_{h\Delta 1} (\varphi^\dagger \varphi) \text{Tr}[\hat{\Delta}^\dagger \hat{\Delta}] + \lambda_{h\Delta 2} (\varphi^\dagger \hat{\Delta} \hat{\Delta}^\dagger \varphi) \\ & + \mu_{h\Delta} (\varphi^\dagger \hat{\Delta} \cdot \varphi^\dagger + \text{H.c.}). \end{aligned} \tag{11}$$

The parameters $\{\lambda\}$ are real dimensionless couplings. The dimensionful parameter $\mu_{h\Delta}$ signifies the scale below which lepton number is not conserved. Under canonical quantum number assignments, SM leptons and antileptons carry lepton numbers $L_{\text{lep}} = +1$ and $L_{\text{antilep}} = -1$, respectively, the SM Higgs carries no lepton number, and $\hat{\Delta}$ carries $L_\Delta = -2$.

The $\varphi - \varphi - \Delta$ term in the third line of Eq. (11), therefore, breaks lepton number symmetry explicitly by two units and induces the following VEV for $\hat{\Delta}$ after EWSB:

$$\sqrt{2} \langle \hat{\Delta} \rangle = v_\Delta \approx \frac{\mu_{h\Delta} v_\varphi^2}{\sqrt{2} m_{\hat{\Delta}}^2}. \tag{12}$$

Here, $v_\varphi = \sqrt{2} \langle \varphi \rangle$ is the VEV of the SM Higgs and we assume $m_{\hat{\Delta}} \gg v_\varphi$. Measurements of M_W in conjunction with the absence of flavor-violating decays of τ and μ leptons require $v_\Delta \gtrsim 10$ eV–1 keV, depending on one's underlying assumptions [22,44–46]. Constraints on v_Δ will be revisited in Sec. II A.

The mass eigenstates of the type II seesaw are those of the SM, with at least two massless neutrinos being replaced by Majorana neutrinos, plus one doubly charged scalar $\Delta^{\pm\pm}$, one singly charged scalar $\Delta^\pm$, one neutral CP-even scalar Δ^0, and one neutral CP-odd scalar ξ^0. For $v_\Delta \ll v_\varphi$, the mass eigenvalues of these scalars obey the sum rule

$$\delta M_\Delta^2 \equiv M_{\Delta^0}^2 - M_{\Delta^\pm}^2 = M_{\Delta^\pm}^2 - M_{\Delta^{\pm\pm}}^2 = \lambda_{h\Delta 2} \frac{v_\varphi^2}{4}, \tag{13}$$

with $M_{\xi^0} \simeq M_{\Delta^0}$. Notice that $\lambda_{h\Delta 2}$ can have either sign, so the triplet hierarchy is not fixed *a priori*: $\Delta^{\pm\pm}$ could be the heaviest or lightest of the components. The new states give rise to a variety of testable predictions at hadron colliders [34,35,47–52]. For recent LHC updates, see Refs. [36,37,43,52–55].

At the LHC, direct searches for type II scalars set stringent constraints but depend on benchmark assumptions and signatures [26–31]. For small v_Δ, the Yukawa couplings are sizable and the doubly charged scalar decays solely to charged leptons. Searches for these golden channels by ATLAS at the 95% confidence level (CL) using run II data exclude $M_{\Delta^{\pm\pm}} < 1080$ GeV [29], rendering the triplet too heavy to resolve the W-mass anomaly. For larger VEVs, the dilepton channels become subdominant compared to the more-involved bosonic decays. In the pair and associated production channels

$$pp \to \Delta^{++} \Delta^{--} \to W^+ W^+ W^- W^-, \tag{14a}$$

$$pp \to \Delta^{\pm\pm} \Delta^{\mp} \to W^\pm W^\pm W^\mp Z, \tag{14b}$$

and for fully leptonic and semileptonic final states, doubly charged scalar masses in the range $M_{\Delta^{\pm\pm}} = 200$–$350$ GeV are excluded by ATLAS at the 95% CL using the full run II dataset [27,28]. This exclusion assumes $v_\Delta = 0.1$ GeV but holds for larger v_Δ. The limits of Ref. [28] are driven by searches for $\Delta^{++}\Delta^{--}$ pair production; limits from searches for $\Delta^{\pm\pm}\Delta^{\mp}$ only exclude $M_{\Delta^{\pm\pm}} < 230$ GeV at 95% CL for $|M_{\Delta^\pm} - M_{\Delta^{\pm\pm}}| < 5$ GeV. A recasting of run I results finds $M_{\Delta^{\pm\pm}} < 84$ GeV excluded [56–58], leaving an allowed region of 84 GeV $< M_{\Delta^{\pm\pm}} < 200$ GeV that is suited to explain the CDF result over a large range of triplet VEVs [22,25].

For intermediate v_Δ, it is possible for light triplet scalars to be so long-lived that they circumvent the prompt-decay limits above. Investigations [59,60] find that this occurs roughly in the triangle in $(M_{\Delta^{\pm\pm}}, v_\Delta)$ space enclosed by the points:

$$(M_{\Delta^{\pm\pm}}, v_\Delta) = (90\ \text{GeV}, 10^{-1}\ \text{GeV}), \tag{15a}$$

$$(M_{\Delta^{\pm\pm}}, v_\Delta) = (90\ \text{GeV}, 10^{-4}\ \text{GeV}), \tag{15b}$$

$$(M_{\Delta^{\pm\pm}}, v_\Delta) = (200\ \text{GeV}, 10^{-4}\ \text{GeV}). \tag{15c}$$

For larger $(M_{\Delta^{\pm\pm}}, v_\Delta)$, $\Delta^{\pm\pm}$ has a characteristic lifetime below the threshold $c\tau_0 = 1$ mm, and is therefore short lived.

We briefly note that the search for Higgs pair production at ATLAS with its full run II dataset [61] has been reinterpreted for the type II seesaw. Specifically, Ref. [24] reports that the absence of an enhanced, loop-induced $H \to \gamma\gamma$ rate in this search leads to $M_{\Delta^{\pm\pm}} \lesssim 250$ GeV being excluded. The values of $(M_{\Delta^{\pm\pm}}, M_{\Delta^\pm})$ that can explain CDF's data, however, lie along the boundary of this reinterpreted limit. This limit is also subject to several uncertainties, including corrections to Higgs pair production, which is assumed to be SM-like.

A. M_W in the type II seesaw at tree level and one loop

At tree level, a nonzero v_Δ formally leads to a Z mass that is larger than predicted in the SM. When M_Z is used as an EW reference point, this manifests as a tree-level W mass that is *smaller* than expected in the SM. From both perspectives, one anticipates a smaller M_W-over-M_Z ratio, which can be quantified by the ρ [18] and oblique (S, T, U) [62,63] parameters:

$$\rho_{\text{tree}} = \frac{M_W^2}{M_Z^2 \cos^2\theta_W} = 1 + \alpha_{\text{EM}} T_{\text{tree}} = 1 - \frac{2v_\Delta^2}{v_\varphi^2 + 2v_\Delta^2}. \tag{16}$$

In the SM, one has $\rho_{\text{tree}} = 1$ and $T_{\text{tree}} = 0$, with deviations in the type II seesaw driven at tree level by v_Δ. Qualitatively, EWPD lead to the condition that $v_\Delta \ll v_\varphi$, even in light of CDF's measurement [21,64,65].

At one loop, contributions to the W boson's self-energy from triplet scalars lead to a shift in its mass that scales with δM_Δ^2. In terms of the oblique parameters S and T, and with $U = 0$ since it is small, such contributions can be expressed as [62,63,66]

$$M_W \approx M_W^{\text{SM}}\left[1 - \frac{\alpha_{\text{EM}}}{4(1-2s_W^2)}(S - 2(1-s_W^2)T)\right], \tag{17}$$

using the shorthand $s_W^2 \equiv \sin^2\theta_W$. For heavy triplet masses, small mass splittings $(\delta M_\Delta^2/M_{\Delta^0}^2)$, and neglecting $\mathcal{O}(v_\Delta^2/v_\varphi^2)$ terms, the one-loop expressions in the type II seesaw are [37]

$$S_{\text{1-loop}} \approx -\frac{(2 - 4s_W^2 + 5s_W^4)M_Z^2}{30\pi M_{\Delta^0}^2} + \frac{2\delta M_\Delta^2}{3\pi M_{\Delta^0}^2}, \tag{18a}$$

$$T_{\text{1-loop}} \approx \frac{(\delta M_\Delta^2)^2}{12\pi^2 \alpha_{\text{EM}} M_{\Delta^0}^2 v_\varphi^2}. \tag{18b}$$

Here, we highlight the distinction between tree-level shifts to M_W, which are driven by the (small) triplet VEV v_Δ, and one-loop shifts, which depend on δM_Δ^2. Due to this difference, it is possible that positive one-loop corrections to M_W (or T) can exceed the negative tree-level correction to M_W [21,22].

Adjusting the W mass in Eq. (17) to match CDF's value from Eq. (1) fixes one linear combination of S and T. Complementary constraints arise from EWPD, notably the weak mixing angle θ_W [24]. A dedicated fit to EWPD including CDF's data finds the best-fit value $(S, T) = (0.17, 0.27)$ [67,68]. That T is positive requires $|T_{\text{1-loop}}| > |T_{\text{tree}}|$, which is naturally achieved for $v_\Delta \ll v$. The positive S furthermore favors $\delta M_\Delta^2 > 0$ within 1σ, and hence favors the mass hierarchy

$$M_{\Delta^{\pm\pm}}^2 < M_{\Delta^\pm}^2 < M_{\Delta^0}^2 \sim M_{\xi^0}^2. \tag{19}$$

The best fit of Ref. [68] translates roughly to the values [22]

$$(M_{\Delta^{\pm\pm}}, M_{\Delta^\pm} - M_{\Delta^{\pm\pm}}) \approx (95.5\ \text{GeV}, 72.5\ \text{GeV}). \tag{20}$$

Using the full expressions at one loop for S, T [62,63] but neglecting tree-level contributions, which are $\mathcal{O}(v_\Delta^2/v_\varphi^2) \ll 1$, Ref. [22] finds that the uncertainty in Eq. (1) corresponds at 1σ to the following (correlated) parameter space that additionally remains unconstrained by direct searches for type II seesaw:

$$1\ \text{MeV} \lesssim v_\Delta \lesssim 1\ \text{GeV}, \tag{21a}$$

$$84\ \text{GeV} < M_{\Delta^{\pm\pm}} < 200\ \text{GeV}, \tag{21b}$$

$$56\ \text{GeV} < M_{\Delta^\pm} - M_{\Delta^{\pm\pm}} < 81\ \text{GeV}, \tag{21c}$$

$$46\ \text{GeV} < M_{\Delta^0} - M_{\Delta^\pm} < 53\ \text{GeV}. \tag{21d}$$

This is the preferred region of parameter space in the type II seesaw (in the natural limit $v_\Delta \ll v_\varphi$) that can reconcile CDF's measurement of M_W with EWPD. For larger v_Δ, i.e., $v_\Delta \gtrsim 1$ GeV, one needs larger mass splittings δM_Δ^2 in order to compensate for the larger, unwanted tree-level contribution to T [21]. In this fine-tuned region, one can also have larger triplet masses than indicated by Eq. (21) in order to keep S small. Since many of our assumptions rely on small v_Δ, which is also the more natural parameter space to explain CDF's finding, we restrict ourselves to the triplet parameter space of Eq. (21). In Sec. IV, we report a test of this parameter space by reinterpreting measurements of SM signatures at the LHC.

III. REINTERPRETING LHC MEASUREMENTS OF SM SIGNATURES

The LHC detector experiments are producing a growing library of measurements of differential cross sections, exploring a wide range of particle final states in pp collisions at $\sqrt{s} = 7$, 8, and 13 TeV collision energies. While the primary motivation for these measurements is to probe the SM itself and test SM predictions in new kinematic regimes, many measurements are made in a sufficiently model-independent fashion that non-SM processes may be "signal injected" onto measured phase spaces. Usually denoted as a "fiducial region," this restriction of phase space implements the experimental analysis cuts on the final-state particles. Thus, the acceptance (and potential discovery/exclusion) for any BSM events populating this volume of phase space can be evaluated.

To carry out this discovery/exclusion procedure, we use a new release (v2.4.0) of the tool CONTUR. CONTUR is a package that exploits the analysis routines published in RIVET (v3.1.6) [69] and YODA (v1.9.6), and which in turn obtains the measurement data from HEPData [70]. In CONTUR, a χ^2 test statistic is used to compare the likelihoods that a given measurement was obtained under competing assumptions, namely that either the SM alone or SM + BSM is the underlying distribution. The likelihood ratio is then used to derive a CL for testing a BSM hypothesis. Correlations between the uncertainties are taken into account where available. More details on CONTUR may be found in Ref. [40].

To simulate signal processes from the type II seesaw at the LHC, we use the public `TypeIISeesaw` libraries of Ref. [43]. These libraries are an implementation of the model described in Sec. II into the FeynRules package [71,72] and are available as a set of Universal FeynRules Object (UFO) libraries [73]. Parton-level matrix elements are computed at lowest order (LO) by importing the above UFO into MGaMC (v2.9.10).

We focus on the production and decay channels

$$pp \to \Delta^{++}\Delta^{--} \to W^{+(*)}W^{+(*)}W^{-(*)}W^{-(*)}, \tag{22a}$$

$$pp \to \Delta^{\pm\pm}\Delta^{\mp} \to W^{\pm(*)}W^{\pm(*)}\Delta^{\pm\pm}W^{\pm(*)} \to 5W^{(*)}, \tag{22b}$$

which are shown graphically in Fig. 1, and which are driven by the $\Delta^{\pm\pm} \to W^{\pm(*)}W^{\pm(*)}$ and $\Delta^{\pm} \to \Delta^{\pm\pm}W^{\mp(*)}$ decay modes.[2] The $W^{(*)}$ are allowed to split into both lepton pairs and quark pairs.

[2]Adding the channel $pp \to \Delta^{\pm}\Delta^{0}$ is computationally expensive and only strengthens the significance of our excluded region. Therefore, we neglect it in our study. We also do not consider interference with SM processes, which is anyway not present for most LHC measurements, since we are considering resonant production of $\Delta^{\pm(\pm)}$ states and signal processes with 4-to-5 $W^{(*)}$ bosons.

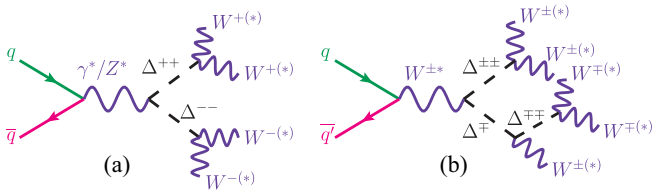

FIG. 1. Graphs illustrating the production of type II scalars in (a) neutral-current and (b) charged-current quark-antiquark annihilation at the Born level and their decays to W bosons (drawn with JAXODRAW [74]).

Matrix elements are convolved with the NNPDF 3.0 LO parton distribution function (lhaid = 263400) [75]. Decays of triplet scalars are treated using the narrow width approximation as implemented into MGaMC's MadSpin module [76,77]. Parton-level events are passed to PYTHIA (v8.306) [78] to simulate showering and hadronization, using the Monash 2013 tune [79]. Multiparton interactions are disabled in order to speed up the simulation process. Finally, a new interface between MGaMC and CONTUR passes the HEPMC outputs of PYTHIA to the RIVET routines for LHC run I and run II measurements.[3]

The above sequence is carried out over the parameter space

$$M_{\Delta^{\pm\pm}} \in [60\ \text{GeV}, 400\ \text{GeV}], \tag{23a}$$

$$\Delta_M \equiv M_{\Delta^{\pm}} - M_{\Delta^{\pm\pm}} \in [35\ \text{GeV}, 155\ \text{GeV}], \tag{23b}$$

which covers the parameter space summarized in Eq. (21). Scalar masses are fixed to obey the sum rule in Eq. (13) and the mass hierarchy in Eq. (19). While the neutral scalars Δ^0, ξ^0 are present in the model, we do not include their contributions since they are heavier and have smaller production cross sections. Additionally, we fix $v_\Delta = 1$ GeV; larger values increase the $\Delta^{\pm\pm} \to W^{(*)}W^{(*)}$ branching ratio, and therefore increase the channel's signal strength. We have checked numerically that this behavior is realized in our simulations.

IV. RESULTS

In Fig. 2, we overlay the $(M_{\Delta^{\pm\pm}}, \Delta_M)$ parameter space we investigate with exclusion limits set by CONTUR. As discussed in Sec. II, doubly charged scalar masses in the range $M_{\Delta^{\pm\pm}} = 84$–200 GeV are not excluded by direct searches by either ATLAS or CMS. The best-fit point for the recent M_W measurement from CDF, and summarized in Eq. (20), lies in this window. We find that the limit from CONTUR excludes all of this window. More specifically, we report that at 95% CL

[3]The full list can be found in the CONTUR 2.4.0 release.

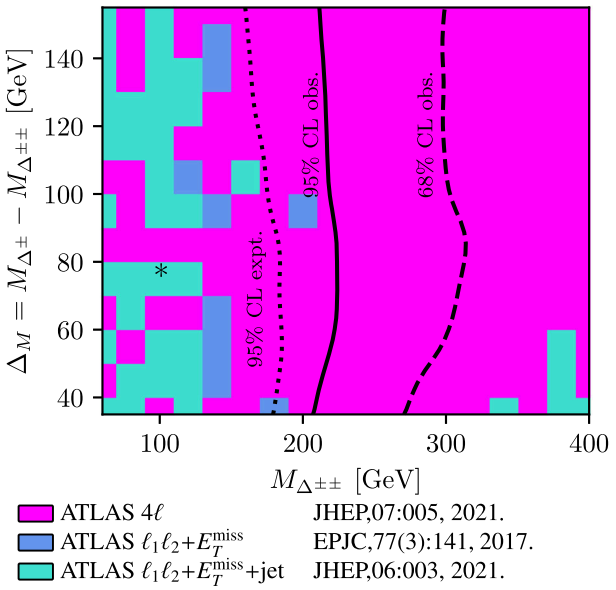

FIG. 2. The $(M_{\Delta^{\pm\pm}}, \Delta_M)$ parameter space overlaid with the 95% (solid) and 68% (long-dashed) exclusion limits as obtained from MGaMC+CONTUR. (Values to the left of the lines are excluded.) Also shown is the 95% expected exclusion (dotted). The color-shading scheme indicates which SM measurement provides the dominant exclusion. The black asterisk indicates the best fit value from [22].

$$M_{\Delta^{\pm\pm}} < 200 \text{ GeV} \quad \text{for } \Delta_M \in [35, 155] \text{ GeV} \tag{24}$$

are excluded by measurements of SM signatures at the LHC. We have checked that these limits extend to larger mass splittings as well, i.e., where $\Delta^\pm$ becomes irrelevant. These limits are obtained for a VEV of $v_\Delta = 1$ GeV and are applicable for larger v_Δ. For smaller v_Δ, experimental acceptance, and hence sensitivity, can degrade due to too-long scalar lifetimes. The analyses here assume triplet scalars decay promptly after production. For further discussion, see Sec. II.

For most of the parameter plane, the exclusion is driven by the inclusive, four-lepton cross section measurement from ATLAS [80], which uses $\mathcal{L} = 139$ fb^{-1} of data at 13 TeV. The search for triboson WWW production from ATLAS at 8 TeV with $\mathcal{L} = 20$ fb^{-1} of data [81] and ATLAS' $WW+$jet measurement at 13 TeV with $\mathcal{L} = 139$ fb^{-1} of data [82] drive the exclusion for parts of the low-$M_{\Delta^{\pm\pm}}$ region.

To explore further the phenomenology driving the expected (dotted) and observed 95% (solid) exclusion limits in Fig. 2, we draw attention to the sensitivity to $M_{\Delta^{\pm\pm}}$ as a function of Δ_M. In the expected limits, there is moderate sensitivity to the mass splitting while the observed limits appear largely insensitive to Δ_M. The observed limits are also somewhat more stringent than the expected limits. The results follow from several competing and complementing factors.

Focusing first on the expected limits at small $M_{\Delta^{\pm\pm}}$ and small Δ_M, one expects comparable signal contributions from the $\Delta^{++}\Delta^{--}$ pair production process in Eq. (22a) and the $\Delta^{\pm\pm}\Delta^{\mp}$ associated production channel in Eq. (22b). This follows from $\Delta^{\pm\pm}\Delta^{\mp}$ production having generically [43] a production cross section that is about $\mathcal{O}(2\times)$ larger than the $\Delta^{++}\Delta^{--}$ production rate combined with the $\Delta^\pm \to \Delta^{\pm\pm} f\overline{f'}$ decay rate reaching $\text{BR}(\Delta^\pm \to \Delta^{\pm\pm} f\overline{f'}) \sim \mathcal{O}(50\%)$. This means that the two channels in Eqs. (22a) and (22b) effectively have the same cross section for small $M_{\Delta^{\pm\pm}}$ and small Δ_M.

As the mass splitting increases, two competing effects in the associate production channel occur: (i) the $\Delta^{\pm\pm}\Delta^{\mp}$ production cross section decreases due to phase space suppression, (ii) the $\Delta^\pm \to \Delta^{\pm\pm} f\overline{f'}$ decay rate increases to $\text{BR}(\Delta^\pm \to \Delta^{\pm\pm} f\overline{f'}) \gtrsim \mathcal{O}(90\%)$ for $M_{\Delta^{\pm\pm}} \gtrsim 60$ GeV due to coupling enhancements. The former occurs faster than the later, leading to the associated production channel effectively turning off for large Δ_M, and which translates to a decrease in expected sensitivity.

Focusing now on the observed limits, we find that the observed limits constrain $M_{\Delta^{\pm\pm}}$ by about 30–50 GeV more than the expected limits. This comes from the fact that (i) the measurements we considered are statistics limited and (ii) the SM prediction lies above the measured data in the most sensitive region of the measurement—the mass distribution of each dilepton pair in the event. An example of such a distribution is presented in Fig. 3, which shows the mass distribution of the highest-mass dilepton pair in 4ℓ events when the four-lepton system has a mass greater than twice the Z mass [80]. Signal events for the representative mass points $(M_{\Delta^{\pm\pm}}, M_{\Delta^\pm}) = (180 \text{ GeV}, 255 \text{ GeV})$ have been injected.

V. OUTLOOK AND CONCLUSION

Among the proposed new physics reasons for the difference between CDF's precision measurement of the W's mass and the SM expectation, the type II seesaw model stands out for having long predicted a shift in the W mass and furthermore for being a realistic scenario to explain neutrino masses. Recent studies [21–23] indicate that in order to accommodate CDF's measurement, triplet scalars must carry masses of few-to-several hundred GeV. This is well within the LHC's kinematic reach. However, due to their sizable decay rates to EW bosons and lighter triplet scalars, direct searches for the scalars $\Delta^{\pm\pm}$ and $\Delta^\pm$ from the type II seesaw have not fully probed this window.

In this study, we exploit the fact that triplet scalars with such properties contribute (at some subleading level) to measurements of SM signatures at the LHC. These include triboson processes, e.g., $pp \to WWW$, and diboson processes, e.g., $pp \to W/Z + nj$, as well as agnostic searches for new physics. Using releases of MGaMC and CONTUR

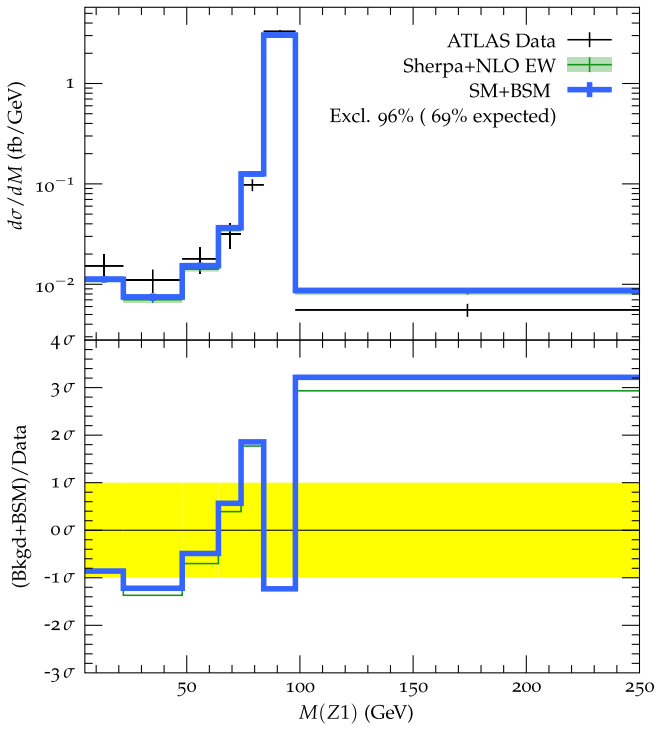

FIG. 3. Upper panel: representative differential cross section as a function of the highest-mass dilepton pair in 4ℓ measurements used in this study showing ATLAS data (crosses) [80], predicted SM yields (green) [83], and predicted SM + BSM yields for $(M_{\Delta^{\pm\pm}}, M_{\Delta^{\pm}}) = (180\ \text{GeV}, 255\ \text{GeV})$ (blue). Lower panel: bin-by-bin significance of expected theory yields relative to data with combined data and theory uncertainties (band).

that interface natively, in conjunction with an updated FeynRules description of the type II seesaw [43], we have performed an analysis of the type II seesaw using publicly available measurements from runs I and II of the LHC.

For promptly decaying $\Delta^{\pm\pm}$, we find that the best-fit point and the 1σ region in the type II seesaw's parameter space consistent with CDF's measurement [22], given in Eqs. (20) and (21) respectively, are already excluded by LHC data at 95% CL, as shown in Fig. 2. This exclusion is driven by precision measurements of triboson and diboson processes at run II. This region was previously unconstrained by direct ATLAS and CMS searches. The remaining parameter space preferred by CDF corresponds to the limit that triplet scalars are long-lived and prompt-decay searches do not apply, and summarized in Eq. (15). We encourage dedicated experimental searches to probe this gap.

Finally, the methodology employed here is applicable to other untested parameter spaces in the type II seesaw (as well as in other models) that feature a collider phenomenology similarly characterized by cascade decays, moderate mass splittings, and many soft final states, i.e., not by golden collider signatures. Since the measurements used here are generally statistically limited, more precise measurements, with greater kinematic coverage, should be a priority for the coming years of high-luminosity running, and will significantly extend the model space which can be probed by these methods.

ACKNOWLEDGMENTS

Benjamin Fuks, Jonathan Kriewald, Miha Nemevšek, and Carlo Tamtam are thanked for helpful discussions. The research activities of J. H. are supported in part by the National Science Foundation under Grant No. PHY-2210428. The work of S. J. is supported by the National Research Foundation of Korea (NRF) Grant funded by the Korean government (NRF-2021R1A2C2014311). O. M. received funding from FRS-FNRS agency via the IISN maxlhc convention (4.4503.16). R. R. acknowledges the support of Narodowe Centrum Nauki under Grant No. 2019/34/E/ST2/00186. The author also acknowledges the support of the Polska Akademia Nauk (Grant Agreement No. PAN.BFD.S.BDN. 613. 022. 2021—PASIFIC 1, POPSICLE). This work has received funding from the European Union's Horizon 2020 research and innovation program under the Skłodowska-Curie Grant Agreement No. 847639 and as part of the Skłodowska-Curie Innovative Training Network MCnetITN3 (Grant Agreement No. 722104), and from the Polish Ministry of Education and Science.

[1] T. Aaltonen *et al.*, High-precision measurement of the W boson mass with the CDF II detector, Science **376**, 170 (2022).
[2] J. de Blas, M. Ciuchini, E. Franco, S. Mishima, M. Pierini, L. Reina, and L. Silvestrini, Electroweak precision observables and Higgs-boson signal strengths in the Standard Model and beyond: Present and future, J. High Energy Phys. 12 (2016) 135.
[3] M. Aaboud *et al.*, Measurement of the W-boson mass in pp collisions at $\sqrt{s} = 7$ TeV with the ATLAS detector, Eur. Phys. J. C **78**, 110 (2018); **78**, 898(E) (2018)].
[4] R. Aaij *et al.*, Measurement of the W boson mass, J. High Energy Phys. 01 (2022) 036.
[5] J. de Blas, M. Ciuchini, E. Franco, A. Goncalves, S. Mishima, M. Pierini, L. Reina, and L. Silvestrini, Global

analysis of electroweak data in the Standard Model, Phys. Rev. D **106**, 033003 (2022).
[6] J. Gao, D. Liu, and K. Xie, Understanding PDF uncertainty on the W boson mass measurements in CT18 global analysis, Chin. Phys. C **46**, 123110 (2022).
[7] S. P. Martin, Three-loop QCD corrections to the electroweak boson masses, Phys. Rev. D **106**, 013007 (2022).
[8] J. Isaacson, Y. Fu, and C. P. Yuan, ResBos2 and the CDF W mass measurement, arXiv:2205.02788.
[9] R. K. Ellis, W. Furmanski, and R. Petronzio, Power corrections to the parton model in QCD, Nucl. Phys. **B207**, 1 (1982).
[10] R. K. Ellis, W. Furmanski, and R. Petronzio, Unraveling higher twists, Nucl. Phys. **B212**, 29 (1983).
[11] J. Collins, *Foundations of Perturbative QCD* (Cambridge University Press, Cambridge, England, 2013), Vol. 32.
[12] W. Konetschny and W. Kummer, Nonconservation of total lepton number with scalar bosons, Phys. Lett. **70B**, 433 (1977).
[13] M. Magg and C. Wetterich, Neutrino mass problem and gauge hierarchy, Phys. Lett. **94B**, 61 (1980).
[14] T. P. Cheng and L.-F. Li, Neutrino masses, mixings and oscillations in $SU(2) \times U(1)$ models of electroweak interactions, Phys. Rev. D **22**, 2860 (1980).
[15] J. Schechter and J. W. F. Valle, Neutrino masses in $SU(2) \times U(1)$ theories, Phys. Rev. D **22**, 2227 (1980).
[16] G. Lazarides, Q. Shafi, and C. Wetterich, Proton lifetime and fermion masses in an SO(10) model, Nucl. Phys. **B181**, 287 (1981).
[17] R. N. Mohapatra and G. Senjanovic, Neutrino masses and mixings in gauge models with spontaneous parity violation, Phys. Rev. D **23**, 165 (1981).
[18] D. A. Ross and M. J. G. Veltman, Neutral currents in neutrino experiments, Nucl. Phys. **B95**, 135 (1975).
[19] L. Lavoura and L.-F. Li, Making the small oblique parameters large, Phys. Rev. D **49**, 1409 (1994).
[20] E. J. Chun, H. M. Lee, and P. Sharma, Vacuum stability, perturbativity, EWPD and Higgs-to-diphoton rate in type II seesaw models, J. High Energy Phys. 11 (2012) 106.
[21] S. Kanemura and K. Yagyu, Implication of the W boson mass anomaly at CDF II in the Higgs triplet model with a mass difference, Phys. Lett. B **831**, 137217 (2022).
[22] J. Heeck, W-boson mass in the triplet seesaw model, Phys. Rev. D **106**, 015004 (2022).
[23] R. Ghosh, B. Mukhopadhyaya, and U. Sarkar, The ρ parameter and the CDF W-mass anomaly: Observations on the role of scalar triplets, arXiv:2205.05041.
[24] H. Bahl, W. H. Chiu, C. Gao, L.-T. Wang, and Y.-M. Zhong, Tripling down on the W boson mass, Eur. Phys. J. C **82**, 944 (2022).
[25] Y. Cheng, X.-G. He, F. Huang, J. Sun, and Z.-P. Xing, Electroweak precision tests for triplet scalars, Nucl. Phys. **B989**, 116118 (2023).
[26] M. Aaboud *et al.*, Search for doubly charged Higgs boson production in multi-lepton final states with the ATLAS detector using proton–proton collisions at $\sqrt{s} = 13$ TeV, Eur. Phys. J. C **78**, 199 (2018).
[27] M. Aaboud *et al.*, Search for doubly charged scalar bosons decaying into same-sign W boson pairs with the ATLAS detector, Eur. Phys. J. C **79**, 58 (2019).
[28] G. Aad *et al.*, Search for doubly and singly charged Higgs bosons decaying into vector bosons in multi-lepton final states with the ATLAS detector using proton-proton collisions at $\sqrt{s} = 13$ TeV, J. High Energy Phys. 06 (2021) 146.
[29] ATLAS Collaboration, Search for doubly charged Higgs boson production in multi-lepton final states using 139 fb^{-1} of proton-proton collisions at $\sqrt{s} = 13$ TeV with the ATLAS detector, Technical Report No. ATLAS-CONF-2022-010 (2022).
[30] S. Chatrchyan *et al.*, A search for a doubly-charged Higgs boson in pp collisions at $\sqrt{s} = 7$ TeV, Eur. Phys. J. C **72**, 2189 (2012).
[31] CMS Collaboration, Search for a doubly-charged Higgs boson with $\sqrt{s} = 8$ TeV pp collisions at the CMS experiment, Technical Report No. CMS-PAS-HIG-14-039 (2016).
[32] T. Han, B. Mukhopadhyaya, Z. Si, and K. Wang, Pair production of doubly-charged scalars: Neutrino mass constraints and signals at the LHC, Phys. Rev. D **76**, 075013 (2007).
[33] P. Fileviez Perez, T. Han, G.-Y. Huang, T. Li, and K. Wang, Testing a neutrino mass generation mechanism at the LHC, Phys. Rev. D **78**, 071301 (2008).
[34] P. Fileviez Perez, T. Han, G.-y. Huang, T. Li, and K. Wang, Neutrino masses and the CERN LHC: Testing type II seesaw, Phys. Rev. D **78**, 015018 (2008).
[35] A. Melfo, M. Nemevsek, F. Nesti, G. Senjanovic, and Y. Zhang, Type II seesaw at LHC: The roadmap, Phys. Rev. D **85**, 055018 (2012).
[36] S. Ashanujjaman and K. Ghosh, Revisiting type-II see-saw: Present limits and future prospects at LHC, J. High Energy Phys. 03 (2022) 195.
[37] S. Mandal, O. G. Miranda, G. Sanchez Garcia, J. W. F. Valle, and X.-J, Xu, Toward deconstructing the simplest seesaw mechanism, Phys. Rev. D **105**, 095020 (2022).
[38] T. Stelzer and W. F. Long, Automatic generation of tree level helicity amplitudes, Comput. Phys. Commun. **81**, 357 (1994).
[39] J. Alwall, R. Frederix, S. Frixione, V. Hirschi, F. Maltoni, O. Mattelaer, H. S. Shao, T. Stelzer, P. Torrielli, and M. Zaro, The automated computation of tree-level and next-to-leading order differential cross sections, and their matching to parton shower simulations, J. High Energy Phys. 07 (2014) 079.
[40] A. Buckley *et al.*, Testing new physics models with global comparisons to collider measurements: The CONTUR toolkit, SciPost Phys. Core **4**, 013 (2021).
[41] J. M. Butterworth, D. Grellscheid, M. Krämer, B. Sarrazin, and D. Yallup, Constraining new physics with collider measurements of Standard Model signatures, J. High Energy Phys. 03 (2017) 078.
[42] M. M. Altakach, J. M. Butterworth, T. Ježo, M. Klasen, and I. Schienbein, Probing a leptophobic top-colour model with cross section measurements and precise signal and background predictions: A case study, arXiv:2111.15406.
[43] B. Fuks, M. Nemevšek, and R. Ruiz, Doubly charged Higgs boson production at hadron colliders, Phys. Rev. D **101**, 075022 (2020).
[44] A. Pich, A. Santamaria, and J. Bernabeu, $\mu^- \to e^- + \gamma$ decay in the scalar triplet model, Phys. Lett. **148B**, 229 (1984).

[45] J. Chakrabortty, P. Ghosh, and W. Rodejohann, Lower limits on $\mu \to e\gamma$ from new measurements on U_{e3}, Phys. Rev. D **86**, 075020 (2012).

[46] Y. Cheng, X.-G. He, Z.-L. Huang, and M.-W. Li, Type-II seesaw triplet scalar effects on neutrino trident scattering, Phys. Lett. B **831**, 137218 (2022).

[47] A. G. Akeroyd and M. Aoki, Single and pair production of doubly charged Higgs bosons at hadron colliders, Phys. Rev. D **72**, 035011 (2005).

[48] F. del Aguila and J. A. Aguilar-Saavedra, Distinguishing seesaw models at LHC with multi-lepton signals, Nucl. Phys. **B813**, 22 (2009).

[49] P. Fileviez Perez, T. Han, and T. Li, Testability of type I seesaw at the CERN LHC: Revealing the existence of the B-L symmetry, Phys. Rev. D **80**, 073015 (2009).

[50] A. G. Akeroyd and H. Sugiyama, Production of doubly charged scalars from the decay of singly charged scalars in the Higgs triplet model, Phys. Rev. D **84**, 035010 (2011).

[51] M. Nemevšek, F. Nesti, and J. C. Vasquez, Majorana Higgses at colliders, J. High Energy Phys. 04 (2017) 114.

[52] Y. Cai, T. Han, T. Li, and R. Ruiz, Lepton number violation: Seesaw models and their collider tests, Front. Phys. **6**, 40 (2018).

[53] R. Padhan, D. Das, M. Mitra, and A. Kumar Nayak, Probing doubly and singly charged Higgs bosons at the pp collider HE-LHC, Phys. Rev. D **101**, 075050 (2020).

[54] J. Gluza, M. Kordiaczynska, and T. Srivastava, Discriminating the HTM and MLRSM models in collider studies via doubly charged Higgs boson pair production and the subsequent leptonic decays, Chin. Phys. C **45**, 073113 (2021).

[55] CMS Collaboration, Seesaw model searches using multi-lepton final states at the HL-LHC, Technical Report No. CMS-PAS-FTR-22-003 (2022).

[56] S. Kanemura, K. Yagyu, and H. Yokoya, First constraint on the mass of doubly-charged Higgs bosons in the same-sign diboson decay scenario at the LHC, Phys. Lett. B **726**, 316 (2013).

[57] S. Kanemura, M. Kikuchi, K. Yagyu, and H. Yokoya, Bounds on the mass of doubly-charged Higgs bosons in the same-sign diboson decay scenario, Phys. Rev. D **90**, 115018 (2014).

[58] S. Kanemura, M. Kikuchi, H. Yokoya, and K. Yagyu, LHC run-I constraint on the mass of doubly charged Higgs bosons in the same-sign diboson decay scenario, Prog. Theor. Exp. Phys. **2015**, 051B02 (2015).

[59] P. S. Bhupal Dev and Y. Zhang, Displaced vertex signatures of doubly charged scalars in the type-II seesaw and its left-right extensions, J. High Energy Phys. 10 (2018) 199.

[60] S. Antusch, O. Fischer, A. Hammad, and C. Scherb, Low scale type II seesaw: Present constraints and prospects for displaced vertex searches, J. High Energy Phys. 02 (2019) 157.

[61] ATLAS Collaboration, Combination of searches for non-resonant and resonant Higgs boson pair production in the $b\bar{b}\gamma\gamma$, $b\bar{b}\tau^+\tau^-$ and $b\bar{b}b\bar{b}$ decay channels using pp collisions at $\sqrt{s} = 13$ TeV with the ATLAS detector, Technical Report No. ATLAS-CONF-2021-052 (2021).

[62] M. E. Peskin and T. Takeuchi, A New Constraint on a Strongly Interacting Higgs Sector, Phys. Rev. Lett. **65**, 964 (1990).

[63] M. E. Peskin and T. Takeuchi, Estimation of oblique electroweak corrections, Phys. Rev. D **46**, 381 (1992).

[64] P. A. Zyla *et al.*, Review of particle physics, Prog. Theor. Exp. Phys. **2020**, 083C01 (2020).

[65] J. de Blas, M. Pierini, L. Reina, and L. Silvestrini, Impact of the Recent Measurements of the Top-Quark and W-Boson Masses on Electroweak Precision Fits, Phys. Rev. Lett. **129**, 271801 (2022).

[66] I. Maksymyk, C. P. Burgess, and D. London, Beyond S, T, and U, Phys. Rev. D **50**, 529 (1994).

[67] C.-T. Lu, L. Wu, Y. Wu, and B. Zhu, Electroweak precision fit and new physics in light of the W boson mass, Phys. Rev. D **106**, 035034 (2022).

[68] P. Asadi, C. Cesarotti, K. Fraser, S. Homiller, and A. Parikh, Oblique lessons from the W mass measurement at CDF II, arXiv:2204.05283.

[69] C. Bierlich *et al.*, Robust independent validation of experiment and theory: Rivet version 3, SciPost Phys. **8**, 026 (2020).

[70] E. Maguire, L. Heinrich, and G. Watt, HEPData: A repository for high energy physics data, J. Phys. Conf. Ser. **898**, 102006 (2017).

[71] N. D. Christensen and C. Duhr, FeynRules—Feynman rules made easy, Comput. Phys. Commun. **180**, 1614 (2009).

[72] A. Alloul, N. D. Christensen, C. Degrande, C. Duhr, and B. Fuks, FeynRules 2.0—A complete toolbox for tree-level phenomenology, Comput. Phys. Commun. **185**, 2250 (2014).

[73] C. Degrande, C. Duhr, B. Fuks, D. Grellscheid, O. Mattelaer, and T. Reiter, UFO—The universal FeynRules output, Comput. Phys. Commun. **183**, 1201 (2012).

[74] D. Binosi, J. Collins, C. Kaufhold, and L. Theussl, JaxoDraw: A graphical user interface for drawing Feynman diagrams. Version 2.0 release notes, Comput. Phys. Commun. **180**, 1709 (2009).

[75] R. D. Ball *et al.*, Parton distributions for the LHC run II, J. High Energy Phys. 04 (2015) 040.

[76] P. Artoisenet, R. Frederix, O. Mattelaer, and R. Rietkerk, Automatic spin-entangled decays of heavy resonances in Monte Carlo simulations, J. High Energy Phys. 03 (2013) 015.

[77] J. Alwall, C. Duhr, B. Fuks, O. Mattelaer, D. G. Öztürk, and C.-H. Shen, Computing decay rates for new physics theories with FeynRules and MadGraph5_AMC@NLO, Comput. Phys. Commun. **197**, 312 (2015).

[78] C. Bierlich *et al.*, A comprehensive guide to the physics and usage of PYTHIA 8.3, arXiv:2203.11601.

[79] P. Skands, S. Carrazza, and J. Rojo, Tuning PYTHIA 8.1: The Monash 2013 Tune, Eur. Phys. J. C **74**, 3024 (2014).

[80] G. Aad *et al.*, Measurements of differential cross-sections in four-lepton events in 13 TeV proton-proton collisions with the ATLAS detector, J. High Energy Phys. 07 (2021) 005.

[81] M. Aaboud *et al.*, Search for triboson $W^{\pm}W^{\pm}W^{\mp}$ production in pp collisions at $\sqrt{s} = 8$ TeV with the ATLAS detector, Eur. Phys. J. C **77**, 141 (2017).

[82] G. Aad *et al.*, Measurements of $W^+W^-+ \geq 1$ jet production cross-sections in pp collisions at $\sqrt{s} = 13$ TeV with the ATLAS detector, J. High Energy Phys. 06 (2021) 003.

[83] E. Bothmann *et al.*, Event generation with Sherpa 2.2, SciPost Phys. **7**, 034 (2019).